Open Access

Performance Modulation for Back-Illuminated AlGaN Ultraviolet Avalanche Photodiodes Based on Multiplication Scaling

Volume 11, Number 3, June 2019

Qing Cai
Qian Li
Mo Li
Yin Tang
Jin Wang
Junjun Xue
Dunjun Chen
Hai Lu
Rong Zhang
Youdou Zheng

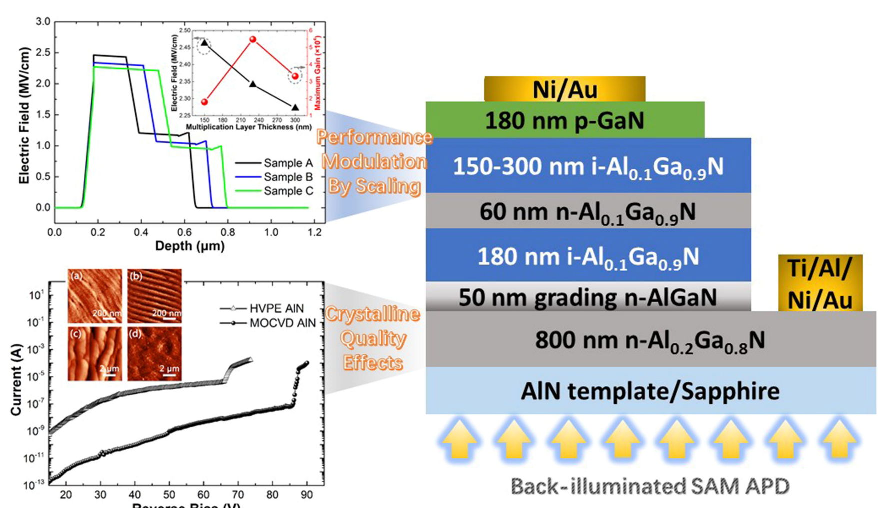

DOI: 10.1109/JPHOT.2019.2914146
1943-0655 © 2019 IEEE

Performance Modulation for Back-Illuminated AlGaN Ultraviolet Avalanche Photodiodes Based on Multiplication Scaling

Qing Cai,[1] Qian Li,[2,3] Mo Li,[2,3] Yin Tang,[1] Jin Wang,[1] Junjun Xue,[4] Dunjun Chen,[1] Hai Lu,[1] Rong Zhang,[1] and Youdou Zheng[1]

[1]Key Laboratory of Advanced Photonic and Electronic Materials, School of Electronic Science and Engineering, Collaborative Innovation Center of Advanced Microstructures, Nanjing University, Nanjing 210093, China
[2]Microsystem and Terahertz Research Center, China Academy of Engineering Physics, Chengdu 610054, China
[3]Institute of Electronic Engineering, China Academy of Engineering Physics, Chengdu 610054, China
[4]School of Electronic Science and Engineering, Nanjing University of Posts and Telecommunications, Nanjing 210023, China

DOI:10.1109/JPHOT.2019.2914146
1943-0655 *© 2019 IEEE. Translations and content mining are permitted for academic research only. Personal use is also permitted, but republication/redistribution requires IEEE permission. See http://www.ieee.org/publications_standards/publications/rights/index.html for more information.*

Manuscript received March 30, 2019; revised April 25, 2019; accepted April 27, 2019. Date of publication April 30, 2019; date of current version May 14, 2019. This work was supported in part by the National Key R&D Program of China under Grant 2016YFB0400903; in part by the National Nature Science Foundation of China (NSFC) under Grant 61634002; in part by the National Natural Science Foundation Committee of China Academy of Engineering Physics Joint Fund (NSAF) under Grant U1830109; in part by the Key R&D Project of Jiangsu Province, China under Grant BE2016174; in part by the Natural Science Foundation of Jiangsu Province under Grant BK20160883; in part by the University Science Research Project of Jiangsu Province under Grant 16KJB140011; and in part by the Scientific Research Foundation of Graduate School of Nanjing University under Grant 2017ZDL02. Corresponding author: Dunjun Chen (e-mail: djchen@nju.edu.cn).

Abstract: Back-illuminated $Al_{0.1}Ga_{0.9}N$ ultraviolet avalanche photodiodes (APDs) of various multiplication widths were fabricated on AlN templates with a separate absorption and multiplication structure. The impacts of an increased multiplication scale on a device performance were investigated. The avalanche breakdown voltage was found to increase as the multiplication layer thickness (MLT) increases. The APD with 230-nm-MLT achieved a superior maximum multiplication gain of 5.4×10^4, higher than that obtained in devices with 150-nm- and 300-nm-MLT. Theoretical simulations demonstrated that the critical electric field intensity in an avalanche region would decrease as the rising of MLT, indicating the modulating ability of multiplication scaling on the AlGaN APD performance. In addition, APDs fabricated on different AlN templates were employed to study the effects of crystalline quality on device properties.

Index Terms: AlGaN, ultraviolet, avalanche photodiodes, multiplication scaling.

1. Introduction

Ultraviolet (UV) avalanche photodiodes (APDs) have plenty of applications in military, scientific, civilian, medical, and biological arenas [1], [2]. As the photomultiplier tubes (PMTs) are fragile, costly and bulky, AlGaN APDs presents themselves as particularly strong candidates for PMTs

because of the high sensitivity and reliability in UV detection [3], [4]. Meanwhile, their properties of direct and wide band gap are superior to silicon and silicon carbide photodetectors due to the ability in intrinsic ultraviolet or solar-blind detecting to replace the optic filters [5]. Current UV APDs based on ZnO and Ga_2O_3 are attracting a large amount of attentions due to their intrinsic band-gaps for UV detection. However, ZnO still faces the challenge of reproducible and stable p-type doping and the avalanche gain of Ga_2O_3 APD is also restricted by the crystal quality [6], [7]. III-nitride based AlGaN alloys are the most promising candidate for UV APD because of the inherent large tunable band-gap and ability to trigger impact ionization to achieve low noise internal gain as well as the mature epitaxy technique. Despite that, AlGaN APDs still retain serious challenges such as lower carrier impact ionization coefficients (IIC) in AlGaN alloys [8]–[10]. In order to enhance the impact ionization, back-illuminated AlGaN APD with separate absorption and multiplication (SAM) structure has been used to yield superior avalanche gain and noise characteristics via impact ionization engineering [11]–[13]. The SAM APDs benefit from initializing impact ionization by nearly pure hole injection into multiplication region and the higher IIC for holes [14]. Back-illuminated designs also favor the packaging and integration of readout circuits by flip-chip bonding. Nevertheless, except for a few simulated reports and p-i-n (Al)GaN APDs, there is still a lack of research on the multiplication region of AlGaN SAM APDs. In this work, we investigated the fabrication and characterization of AlGaN SAM APDs based on the multiplication scaling. Meanwhile, APDs grown on different AlN templates were also employed to study the effects of crystalline quality on device properties.

2. Methods

The growth of APD samples were carried out by metal-organic chemical vapor deposition (MOCVD) reactor, using trimethylgallium (TMGa) and trimethylaluminum (TMAl) as metal precursors while ammonia (NH_3) as the nitrogen source, respectively. P- and n-type doping were carried out with Cp_2Mg and SiH_4, respectively. 500-nm-thick AlN template grown by MOCVD and 9-μm-thick AlN template grown by hydride vapor phase epitaxy (HVPE) were both employed to manufacture SAM structure to study the effect of distinct templates on device performance. The essential device structure consists of an n-type ohmic contact layer of 800-nm-thick $Al_{0.2}Ga_{0.8}N$, a 50-nm-thick n-type AlGaN layer with grading Al composition for reducing negative polarization and lattice mismatch, an unintentionally doped 180-nm-thick $Al_{0.1}Ga_{0.9}N$ absorption layer, an n-type $Al_{0.1}Ga_{0.9}N$ interlayer of 60 nm thickness for modulating electric field distribution, an unintentionally doped $Al_{0.1}Ga_{0.9}N$ multiplication layer (varying thickness: 150, 230 and 300 nm), followed by p-type GaN cap layer for ohmic contact of 180 nm thickness. Hall-effect measurement was carried out to test carrier concentrations in these layers, yielding values in the 1×10^{16}, 1×10^{18}, 5×10^{17} and 2×10^{18} for the electron concentrations in the i-$Al_{0.1}Ga_{0.9}N$, n-$Al_{0.1}Ga_{0.9}N$, n-grading-AlGaN and n-$Al_{0.2}Ga_{0.8}N$ layers, respectively, and 1×10^{18} for the hole concentration in the p-GaN layer.

The Ti/Al/Ni/Au (30/150/50/100 nm) were deposited for ohmic contact on the n-$Al_{0.2}Ga_{0.8}N$ layer and annealed at 800 °C for 30 s in N_2 ambient, followed by the deposition of Ni/Au (20/20 nm) on p-GaN ohmic contact layer and annealed at 500 °C for 10 min in air ambient. In addition, the APDs were carried out with a double-mesa processing by photolithography and ICP-RIE etching to suppress the leakage current and reduce the electrical field intensity on the sidewall of APDs, referring to our previous work [15], [16]. Finally, passivation layer of SiO_2 was deposited by PECVD and windows were opened for testing. Sample A, sample B and sample C represent for the devices fabricated on the 500-nm-thick AlN templates while sample D, sample E and sample F represent for the devices fabricated on the 9-μm-thick AlN templates with multiplication layer thickness (MLT) of 150, 230, 300 nm, respectively.

3. Results and Discussions

Optical transmission measurements were carried out under the back-illuminated condition by Ocean Optics DH-2000-BAL (Light source) and NanoCalc-XR for sample A, B and C, as shown in Fig. 1. It can be seen that there are dielectric losses of 20% at the interface between substrate and the

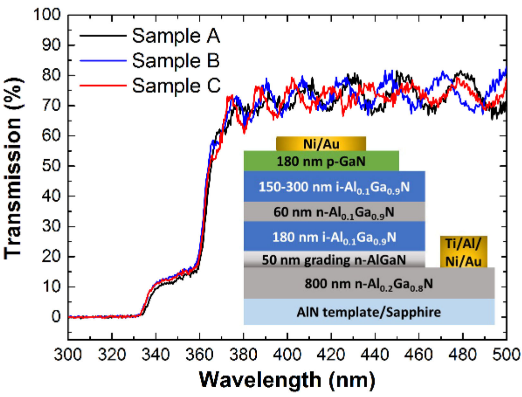

Fig. 1. Transmission spectrum of sample A, B and C. The inset shows the schematic APD structure.

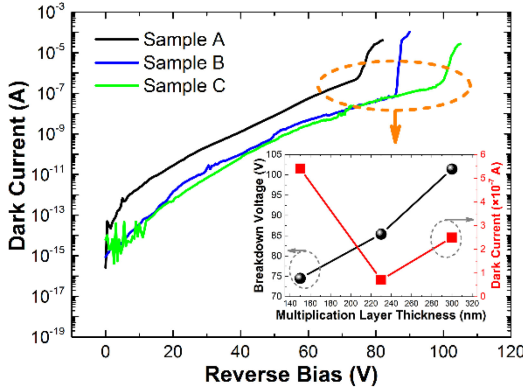

Fig. 2. I-V characteristics of sample A, B and C in the dark. The inset is the onset of V_{br} (black) and dark current at V_{br} (red) versus MLT, respectively.

ambient air. The falling edge at 365 nm corresponds to GaN absorption. Meanwhile, a significant drop is also figured out at 340 nm, indicating the UV absorption by $Al_{0.1}Ga_{0.9}N$ alloy.

A Keithley 4200 semiconductor analyzer and a cascade probe station were used to carry out the I-V measurements. Fig. 2 presents the I-V characteristics of sample A, B and C in dark configuration. The avalanche breakdown of these samples initiates at 74.5, 85.4 and 101.4 V, respectively. As the width of the multiplication region increases, the device needs a higher reverse bias to reach the critical electric field, which accounts for the increasing avalanche breakdown voltage (V_{br}). In addition, at the same reverse bias, the APD of thinner MLT exhibits higher dark currents. This is attributed to the higher electric field intensity and narrower band-gap in multiplication region for thin-MLT device, which leads to higher band-to-band tunneling (BBT) currents. However, the dark current of sample C (2.5×10^{-7} A) is larger than that of sample B (7×10^{-8} A) at the onset of V_{br}. The increase of applied avalanche breakdown voltage will raise the dark current resulted from the surface and sidewall leakage as well as the recombination current. Therefore, it is necessary to comprehensively take the effects of different dark current mechanisms into account in the device design.

To further investigate the impacts of multiplication widths on device performance, I-V curves were also performed under back illumination (at 330 nm) by a fiber-guided UV LED. As shown in Fig. 3(a) for sample B, the light current increases gently and presents a significant uptrend at 84 V. The avalanche process resulted from light current plays a dominant role compared with dark current.

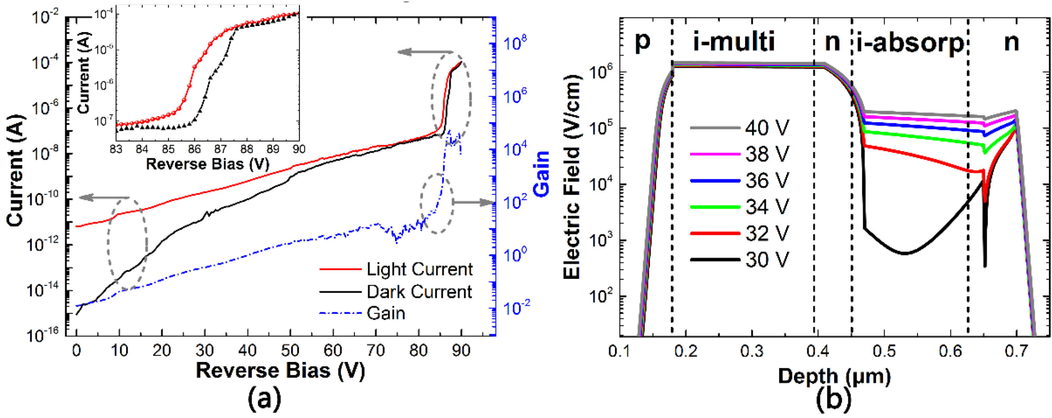

Fig. 3. (a) I-V characteristics of sample B in the dark and UV light, right axis for gain. The inset shows the enlarged IV curves at breakdown voltage; (b) The electric field distribution in sample B with reverse bias ranging from 30 to 40 V.

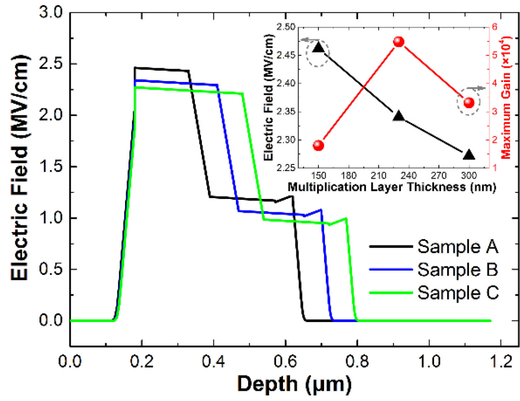

Fig. 4. Calculated electric field distributions at V_{br} for sample A, B and C, respectively. The inset presents the electric field intensity at V_{br} and maximum gain versus MLT.

As the applied voltage increases, the tendency of breakdown curves for both currents become flat due to the threshold energy of carriers and saturation of the impact ionization rate.

The avalanche gain is defined as the difference between the primary multiplied light current and the multiplied dark current, normalized by the difference between the primary unmultiplied light current and the unmultiplied dark current. The unmultiplied currents were calculated at the applied voltage of 40 V for sample B. Numerical calculation for electric field distribution of the fabricated devices was taken by the Silvaco TCAD. The Fig. 3(b) demonstrates that sample B has been punched through when the applied voltage reaches 36 V. Hence, the current difference evaluated at 40 V can ensure that impact ionization has occurred. It can be observed that the gain significantly increases near the onset of breakdown and sample B achieves a superior maximum multiplication gain of 5.4×10^4 (see Fig. 3). The light currents of sample A and C were also measured under the same condition. The inset of Fig. 4 presents that the maximum gain of sample A and C are of 1.8×10^4 and 3.3×10^4, respectively. In order to investigate the change of gain with different multiplication widths, Fig. 4 illustrates the electric field distributions at V_{br} for these samples. It indicates that the rising of MLT will result in decreasing of critical electric field intensity in avalanche region due to stronger photon scattering. Hence, the ionization coefficient of hole tends to decrease with thickening MLT. Meanwhile, as the MLT increases, the carriers can travel farther before reaching the other side of the impact ionization region and thus can contribute more multiplication events [17].

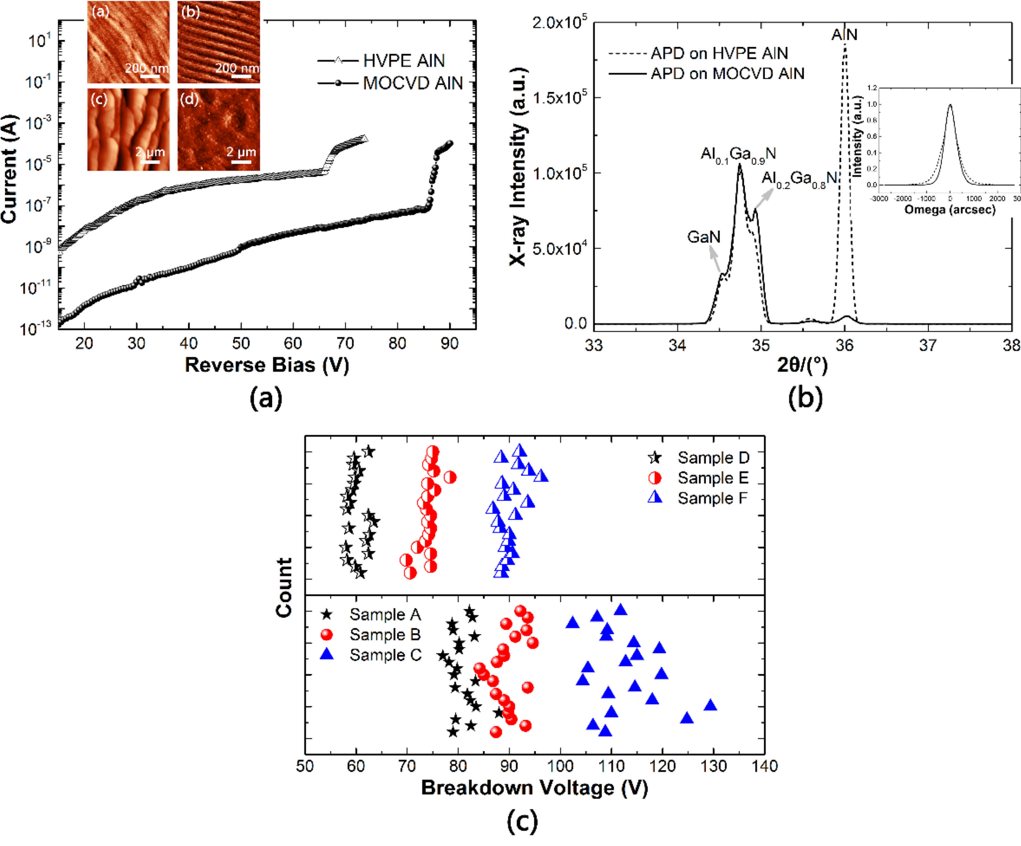

Fig. 5. (a) I-V curves for sample E grown on 9-μm-thick HVPE AlN template (triangle) and sample B grown on 500-nm-thick MOCVD AlN template (circle), respectively; The inset shows AFM microscopic surface morphology of HVPE AlN (a) and MOCVD AlN (b), of sample E (c) and sample B (d), respectively; (b) X-ray diffraction pattern of the sample B and E. The inset presents the (0002) ω-scan rocking curves for $Al_{0.1}Ga_{0.9}N$; (c) Statistics on breakdown voltage of the fabricated samples.

Consequently, there is a tradeoff between hole ionization coefficient and events theoretically, and the shape of maximum gain versus MLT presents a tendency from rise to decline (inset of Fig. 4). These findings also indicate the modulated ability of multiplication scaling on the APD performance.

In order to investigate the effects of crystalline quality on device properties, the 9-μm-thick and 500-nm-thick AlN templates were employed for the SAM structure epitaxy. The microscopic surface of the 500-nm-thick AlN template exhibits a typical step-flow morphology with the root-mean-square surface roughness (RMS) values of 0.118 for the 1×1 μm^2 scan, as shown in the inset (b). The 9-μm-thick AlN template exhibits some voids and dislocations located on the surface with the RMS value of 0.253 for the 1×1 μm^2 scan. Different templates lead to significant discrepancies in the surface morphology of the APDs, as shown in the inset (c) and (d), revealing sample E and B with RMS value of 6.478 and 0.425 for the 5×5 μm^2 scan, respectively. The X-ray diffraction measurement was also carried out to further investigate the crystal quality of the bulk films in Fig. 5(b). As shown in the XRD pattern, $Al_{0.1}Ga_{0.9}N$ in the main functional region of the APD exhibits a distinct peak. The discrepancy in the AlN intensity is ascribed to the thickness gap of AlN templates. Sample B fabricated on 500-nm-thick AlN achieves a (0002) FWHM value of 576 arcsec for $Al_{0.1}Ga_{0.9}N$, which is lower than that of sample E with 637 arcsec. It indicates that different AlN templates will influence crystalline quality of the epitaxial AlGaN alloys. Due to the difference in crystal quality, the dark current of sample B is nearly four orders of magnitude lower than that of sample E [see Fig. 5(a)].

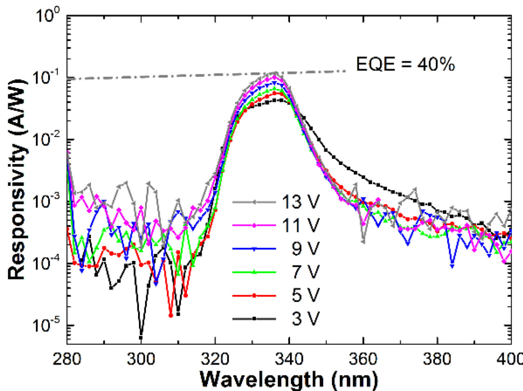

Fig. 6. Spectral responsivity of the APD with different applied voltages.

Meanwhile, both samples demonstrate different breakdown voltages, kept with the same multiplication width though. Furthermore, in order to guarantee the reliability and rationality of the results, twenty devices for each type of sample were taken for statistics on breakdown voltage. Fig. 5(c) indicates that premature breakdown tends to occur in the devices fabricated on the 9-μm-thick AlN template with lower crystalline quality. The mean values of V_{br} for sample A, B and C are of 81, 89.8 and 112.6 V, respectively. The fluctuation is attributed to the difference in dry etching rate of wafers and the non-uniformity of dislocations during epitaxy process.

Fig. 6 presents the spectral responsivity of sample B measured at different reverse applied voltages under back illumination by using a calibrated monochromator and a Xe arc lamp as the light source. A calibrated silicon was employed to measure the power of the monochromatic light. The spectral responsivity of the fabricated APD exhibits a sharp cutoff tendency at the wavelength of 340 nm. A responsivity peak can be observed at 336 nm so as to verify the ultraviolet detecting ability of the APDs, which is in good agreement with the transmission spectrum. As the applied reverse bias reaches 13 V, the peak responsivity of APD can be improved to 0.12 A/W, corresponding to the external quantum efficiency of 40%.

4. Conclusion

In summary, back-illuminated AlGaN SAM APDs with different multiplication scales were fabricated and investigated. A superior maximum multiplication gain of 5.4×10^4 was achieved in the APD with 230-nm-thick multiplication layer, indicating there is a tradeoff in multiplication widths. Breakdown voltage demonstrates a rising tendency with the increasing multiplication widths. In addition, different AlN templates were employed to grow the SAM structure and found that the low crystalline quality would raise dark current of the APD and be easier to trigger premature breakdown. These findings are beneficial for researchers to design and fabricate the AlGaN APDs.

References

[1] R. McClintock, J. L. Pau, K. Minder, C. Bayram, P. Kung, and M. Razeghi, “Hole-initiated multiplication in back-illuminated GaN avalanche photodiodes,” *Appl. Phys. Lett.*, vol. 90, no. 14, 2007, Art. no. 141112.
[2] P. Kung, R. McClintock, J. L. P. Vizcaino, K. Minder, C. Bayram, and M. Razeghi, “III-Nitride avalanche photodiodes,” *Proc. SPIE*, vol. 6479, 2007, Art. no. 64791J.
[3] H. Wu *et al.*, “All AlGaN epitaxial structure solar-blind avalanche photodiodes with high efficiency and high gain,” *Appl. Phys. Exp.*, vol. 9, no. 5, 2016, Art. no. 052103.
[4] Z. Vashaei, E. Cicek, C. Bayram, R. McClintock, and M. Razeghi, “GaN avalanche photodiodes grown on m-plane freestanding GaN substrate,” *Appl. Phys. Lett.*, vol. 96, no. 20, 2010, Art. no. 201908.
[5] J. L. Pau *et al.*, “Geiger-mode operation of back-illuminated GaN avalanche photodiodes,” *Appl. Phys. Lett.*, vol. 91, no. 4, 2007, Art. no. 041104.

[6] J. Yu, C. X. Shan, X. M. Huang, X. W. Zhang, S. P. Wang, and D. Z. Shen, "ZnO-based ultraviolet avalanche photodetectors," *J. Phys. D, Appl. Phys.*, vol. 46, no. 30, Jul. 2013, Art. no. 305105.
[7] B. Zhao *et al.*, "Solar-blind avalanche photodetector based on single ZnO-Ga2O3 core-shell microwire," *Nano Lett.*, vol. 15, no. 6, pp. 3988–3993, Jun. 2015.
[8] Z. G. Shao *et al.*, "Ionization-enhanced AlGaN heterostructure avalanche photodiodes," *IEEE Electron Device Lett.*, vol. 38, no. 4, pp. 485–488, Apr. 2017.
[9] J. Kim *et al.*, "Comparison of AlGaN p-i-n ultraviolet avalanche photodiodes grown on free-standing GaN and sapphire substrates," *Appl. Phys. Exp.*, vol. 8, no. 12, Dec 2015, Art. no. 122202.
[10] H. D. Sun, J. Yin, E. F. Pecora, L. Dal Negro, R. Paiella, and T. D. Moustakas, "Deep-ultraviolet emitting AlGaN multiple quantum well graded-index separate-confinement heterostructures grown by MBE on SiC substrates," *IEEE Photon. J.*, vol. 9, no. 4, Aug 2017, Art. no. 2716420.
[11] Z. Shao *et al.*, "Significant performance improvement in AlGaN solar-blind avalanche photodiodes by exploiting the built-in polarization electric field," *IEEE J. Sel. Topics Quantum Electron.*, vol. 20, no. 6, pp. 187–192, Nov./Dec. 2014.
[12] X. D. Wang *et al.*, "Study of gain and photoresponse characteristics for back-illuminated separate absorption and multiplication GaN avalanche photodiodes," *J. Appl. Phys.*, vol. 115, no. 1, Jan. 2014, Art. no. 013103.
[13] J. Kim *et al.*, "AlxGa1-xN ultraviolet avalanche photodiodes with avalanche gain greater than 10(5)," *IEEE Photon. Technol. Lett.*, vol. 27, no. 6, pp. 642–645, Mar. 2015.
[14] Y. Huang *et al.*, "Back-illuminated separate absorption and multiplication AlGaN solar-blind avalanche photodiodes," *Appl. Phys. Lett.*, vol. 101, no. 25, Dec. 2012, Art. no. 253516.
[15] Z. G. Shao *et al.*, "High-gain AlGaN solar-blind avalanche photodiodes," *IEEE Electron Device Lett.*, vol. 35, no. 3, pp. 372–374, Mar. 2014.
[16] Q. Cai *et al.*, "AlGaN ultraviolet avalanche photodiodes based on a triple-mesa structure," *Appl. Phys. Lett.*, vol. 113, no. 12, Sep. 2018, Art. no. 123503.
[17] J. J. Wanyan, Z. Q. Sun, S. W. Shi, M. Z. Wu, G. He, and G. Li, "Dependence of electrical field and photoresponse on multiplication region thickness for GaN APDs," *Opt. Quantum Electron.*, vol. 46, no. 10, pp. 1297–1301, Oct 2014.